Spin-phonon coupling and magnon scattering in few-layer antiferromagnetic $FePS_3$

Anudeepa Ghosh,[1] Mainak Palit,[1] Sujan Maity,[1] Vivek Dwij,[2] Sumesh Rana,[2] and Subhadeep Datta[1,*]

[1]*School of Physical Sciences, Indian Association for the Cultivation of Science, 2A & B Raja S. C. Mullick Road, Jadavpur, Kolkata 700032, India*

[2]*UGC-DAE Consortium for Scientific Research, University Campus, Khandwa Road, Indore 452001, India*

(Received 28 August 2020; revised 6 January 2021; accepted 15 February 2021; published 25 February 2021)

Temperature-dependent Raman spectroscopic studies of spin-phonon (SP) coupling and magnon scattering in bulk and few-layer (FL) antiferromagnet (AFM) $FePS_3$ with Néel temperature (T_N) $\approx$ 120 K were performed. Bulk and FL (2–5 atomic layers) samples show four distinct modes at room temperature between 150 and 400 cm^{-1} and a broad peak at $\approx$105 cm^{-1}. On lowering the temperature, three distinct phenomena are observed. First, we see the SP coupling, identified by the deviation from the usual two- or three-phonon anharmonic behavior of the higher wave number peaks ($\geqslant$150 cm^{-1}) at or below T_N. The strength of SP coupling can be calculated for bulk and FL flakes considering mean-field approximations. Secondly, we see the spin ordering marked by the evolution of three peaks at lower wave numbers (around 105 cm^{-1}) below T_N due to incommensurate magnetic cells at low temperature. Thirdly, magnon excitation in FL pristine $FePS_3$ is detected by the emergence of a distinct peak at 120 cm^{-1} ($\sim$3.6 THz) at a temperature much lower than T_N ($\approx$60 K). Tracking the magnon mode in the designed van der Waals heterostructures with Bi_2Te_3 and $Cr_2Ge_2Te_6$ reveal interfacial electron and hole transfer from $FePS_3$, respectively. Raman spectroscopy can thus predict the magnetic transition temperature of FL magnetic insulators *via* SP coupling, zone-boundary phonons, and magnons. Quasi-two-dimensional AFMs and their heterostructures involving different electronic and magnetic orders may be promising candidates for ultrafast magnon transport involving magnetoelastic waves.

DOI: 10.1103/PhysRevB.103.064431

I. INTRODUCTION

The Mermin-Wagner theorem restricts long-range magnetic order at finite temperature in a two-dimensional (2D) isotropic ferromagnet [1,2]. However, magnetic anisotropy can counter the thermal fluctuations and lift this restriction, thus leading to magnetism in 2D [1,3]. Magnetism in thin films has been well studied *via* techniques such as magnetic circular dichroism (MCD) and magneto-optical Kerr effect (MOKE) [4]. Ultrathin films of Co, Ni, and Fe reveal larger MCD asymmetries when they are magnetized in the perpendicular direction than the in-plane case due to different spin polarization in these two directions [5]. In spite of being a potential candidate for device application, such thin-film magnetism has been limited by various perturbations, such as reduction of coordination due to band narrowing and atomic diffusion into substrate, effects of strain, and formation of islands [6]. The advent of graphene [7] and 2D semiconductors opened up the possibility of having pristine 2D systems. Initial attempts to develop 2D magnetic systems were limited to doping of graphene [8] and 2D semiconductors like molybdenum disulfides (MoS_2) [9], but such magnetism in the absence of interaction between charge carriers and magnetic moment is uncontrollable and weak (one magnetic moment per 1000 atoms for graphene with adatoms [6]). On the other hand, bulk van der Waals (vdW) magnetic materials such as CrI_3, $Cr_2Ge_2Te_6$, and transition metal phosphorus trisulfides (MPS_3, M = transition metal) well reveal magnetic anisotropy and have been studied *via* superconducting quantum interference devices (SQUIDs) and neutron scattering [10–12].

However, magnetism in an atomically thin sample was initially observed in monolayer CrI_3 *via* polar MOKE, which showed Ising ferromagnetism with out-of-plane spin orientation [13]. In addition, the study also revealed that the substrate effects are weak, and the atomic layers can be regarded as isolated magnets. A concurrent scanning MOKE study revealed pristine $Cr_2Ge_2Te_6$ atomic layers possess intrinsic long-range ferromagnetic (FM) order [14]. Interestingly, magnetism in bilayer CrI_3 could be controlled *via* small gate voltage, and MCD microscopy showed large linear magnetoelectric (ME) effect with reversible electric field switching between interlayer antiferromagnetic (AFM) and FM coupling [15]. Again, in monolayer Fe_3GeTe_2 (FGT) flakes on gold substrate, ferromagnetism with strong perpendicular anisotropy is observed *via* polar reflective MCD and MOKE microscopy [16]. However, Curie temperature was seen to drop to 130 K in monolayer as compared with 207 K in bulk [16,17].

On the other hand, the robustness of T_N in the exfoliated layers of $FePS_3$, which was earlier reported in Ref. [18] and also verified in our experiments, makes these systems an appealing candidate for device applications since T_N remains almost constant with thinning. In addition, nontrivial spin-texture in such 2D systems usually show large anomalous Hall effect with small magnetic field which can be important for topological spintronic devices [19,20]. In terms of

*sspsdd@iacs.res.in

characterization of few-layer (FL) flakes, Kerr effect and MCD have limitations, as the sensitivity of the probes heavily depend on the excitation wavelength, interference, and the thickness of the film [21]. As an alternative, Raman spectroscopy has been a versatile tool to identify layer numbers and study the effects of electric or magnetic perturbations, doping, and disorders in 2D materials [22,23]. Evolution of electronic bands with layer number (N) and the effects of interlayer coupling lead to the change in the Raman-active phonon modes [24]. In context, Raman spectroscopy has been used as an indirect, nondestructive method of probing magnetic ordering in 2D magnetic systems as a function of layer number. In addition, it also provides the energy scales of the spin excitations and phonon modes which can be used to correlate the electron or magnetotransport measurements [25–28]. Though the evolution of layer-dependent magnetic ordering has been studied [29–32], there is no single report that properly classifies all the individual Raman peaks so as to give an entire picture of the Raman spectra of $FePS_3$.

In this paper, we report the systematic study of the Raman signatures of layer-dependent spin-phonon (SP) coupling, spin-dependent Raman scattering, and magnon in bulk and FL flakes of $FePS_3$. On lowering the temperature, the Raman spectra show three distinct phenomena. First, we see SP coupling in higher wave number peaks ($\geqslant 150$ cm^{-1}), where respective vibrational modes show deviation from the anharmonic behavior usual to the optical phonon modes. The onset of deviation corresponds to the AFM transition temperature, and the strength of the SP coupling can be calculated for bulk and FL flakes considering mean-field approximations. Second, we see the evolution of three zone-folded phonon (ZP) modes below T_N from the broad hump at 105 cm^{-1}. This occurs due to doubling of the crystallographic cell into a magnetic superstructure at low temperature, reported earlier in multiferroic systems [33]. Unlike two ZP modes, as reported in Ref. [29], our result shows the appearance of three modes [30,46]. Thirdly, we see the emergence of a one-magnon mode at 120 cm^{-1} in the FL system at a temperature which is lower than T_N ($T_M \sim 60$ K). Tracking the magnon mode in two different vdW heterostructures involving Bi_2Te_3 and $Cr_2Ge_2Te_6$ indicates the electron and hole transfer out of $FePS_3$ at the interface, respectively. Overall, these observations can be useful in (i) fundamental aspects such as the interplay of AFM and superconductivity (SC) where spin-dependent zone-boundary phonons can testify electron-phonon coupling, and (ii) applications, such as ultrafast spintronics and data processing, where magnons as information carriers are coupled to lattice dynamics of the magnetic crystal.

II. SAMPLE PREPARATION AND MEASUREMENT

Commercially available $FePS_3$ (from 2D Semiconductors) was micromechanically exfoliated from the bulk crystal by the standard scotch tape method and transferred onto 285 nm SiO_2 on Si substrate. Suitable flakes were located using Optical Microscope (Olympus BX51) by comparing the transparency of the flakes [Fig. 1(a)]. Thickness measurements were done using atomic force microscopy (Asylum Research) in tapping mode (not shown here). For the proper determination of layer number, we have measured the absorbance of the targeted flakes of $FePS_3$ *via* laser scanning confocal microscopy and correlated the results with the intensity ratio of characteristic Raman peaks, SP3 and SP2 (discussed later in detail) [Fig. 1(d)]. As the layer number decreases, the intensity ratio decreases, which in turn helps us to confirm the layer number from atomic force microscopy data. Henceforth, "FL" samples mean flakes which have a thickness between 2 and 4 nm (≈3–6L), and "bulk" means flakes that have a thickness of >20 nm. Room temperature Raman spectroscopy was done to confirm the phonon modes reported previously in the literature [29,30] [Fig. 1(b)]. Magnetic susceptibility (SQUID, Quantum Design) measurements for the bulk samples were done to confirm the AFM nature ($T_N = 118$ K) with perpendicular anisotropy [Fig. 1(c)]. Note that vdW heterostructures with bulk Bi_2Te_3 and $Cr_2Ge_2Te_6$ (both commercially procured from 2D Semiconductors) were prepared on the same substrate with FL $FePS_3$ flake on top *via* micromanipulation following the stamping method (inset of Fig. 7) as detailed in Ref. [34].

Here, $FePS_3$ has a monoclinic structure, where the Fe atoms form a honeycomb lattice [29]. The structure and spin

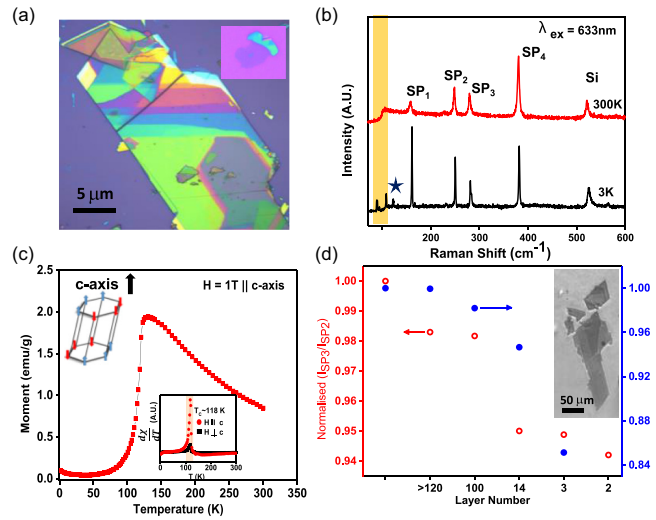

FIG. 1. Iron phosphorus trisulfide ($FePS_3$): (a) Optical contrast image of an exfoliated flake on SiO_2/Si wafer with varying layer number. Inset shows a few-layer flake of lateral dimension ∼5 μm. (b) Room temperature and low temperature Raman spectra ($\lambda_{ex} \sim$ 633 nm) showing the different phonon modes. The shaded region denotes the zone-folded phonon (ZP) modes, the starred peak is the magnon, and the spin-phonon (SP) coupled modes are the peaks denoted by SP1–SP4. SP1 is A_g-B_g mode, SP2 is A_g mode, SP3 is A_g-B_g mode, and SP4 is A_g mode [30]. (c) Temperature-dependent magnetization (M vs T) plot. The antiferromagnetic transition is observed around 118 K (T_N). Magnetic field ($H = 1$ T) was applied along the c axis. The inset on the top shows the spin structure of Fe atoms [48], and the inset at the bottom shows the temperature derivative of magnetic susceptibility for the in-plane and out-of-plane magnetic field, depicting transition temperature with perpendicular anisotropy. (d) Thickness dependence of the intensity ratio of the two characteristic Raman peaks SP3 and SP2. Absorbance of various flakes with different thicknesses, recorded *via* laser scanning confocal microscopy can be correlated to Raman intensity ratio.

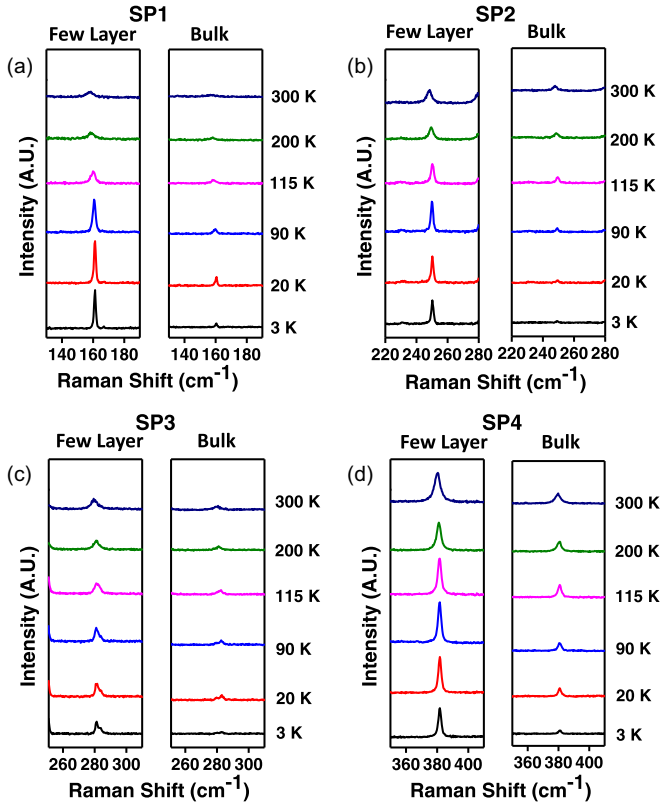

FIG. 2. The evolution of spin-phonon (SP) coupled peaks (a)–(d) SP1–SP4, respectively, from 3 to 300 K. In (a)–(d), the left panel denotes few-layer and the right panel denotes bulk $FePS_3$ flakes. The SP peaks for the few-layer flakes show much larger intensity as compared with the corresponding bulk peaks.

configuration is shown in Fig. 1(c). The spins align AFM in the b and c directions and FM along the a direction. Pre-identified flakes were located using the optical microscope of the Raman setup at room temperature. Note that FL flakes of $FePS_3$ are air-stable for at least 1 month, as confirmed by the continuous tracking of Raman modes. Low temperature Raman spectroscopy was done using the Horiba LabRAM-HR spectrometer with a He-Ne 632.8 nm laser source for a temperature range of 3–300 K. All measurements were performed under high vacuum (10^{-6} mbar) using a liquid helium cryostat (Janis ST-500). Laser beam was focused through a microscope objective with 50× magnification and a spot size of ≈1 μm. Laser power was kept below 200 μW to avoid sample heating.

III. RESULTS AND DISCUSSION

At room temperature, Raman scattering shows distinct peaks at 160 cm^{-1} (SP1), 250 cm^{-1} (SP2), 285 cm^{-1} (SP3), 380 cm^{-1} (SP4), and a broad peak at ≈105 cm^{-1} [Fig. 1(b)]. Careful observation shows that the peaks SP1–SP4 are blueshifted with decreasing temperature [Fig. 2(a)–2(d)]. These peaks show evidence of SP coupling (marked as SP) and vary with flake thickness, which shall be discussed in detail in Sec. III A. On lowering the temperature, three more peaks abruptly appear at or below T_N at 108, 95, and 88 cm^{-1} out of the broad peak at 105 cm^{-1}. These peaks become sharp and distinct with decreasing temperature, and their intensity increases. However, unlike the SP peaks, there is no significant change in their peak positions with decreasing temperature [see Sec. III B]. Around 60 K, a nonintuitive peak appears at 122 cm^{-1} which has been identified as an AFM magnon mode and will be discussed in Sec. III C.

A. Spin-coupled phonons

Figures 2(a)–2(d) show the SP coupled peaks for FL (left panel) and bulk (right panel) samples. The peak intensity of the bulk samples are found to be much less than the FL samples. Note that, except SP3, all peaks (SP1–2, SP4) are shifted to higher energy due to thinning. This might be because the SP3 mode, unlike the rest of the SP modes, has in-plane vibrational nature, as previously reported in Refs. [29,30]. The overall consistency with the theoretical predictions for the bulk samples can be confirmed due to weak interaction between layers [35]. The peaks show blueshift in the range 1–3.2 cm^{-1} with decreasing temperature for the FL and up to 1.2–3 cm^{-1} for bulk in the given window. The plots were fit with the Boltzmann-Sigmoidal equation, which describes the anharmonic dependence of phonon frequency in a given lattice [36]:

$$\omega(T) = \omega_1 + \frac{\omega_0 - \omega_1}{1 + \exp\frac{T - T_0}{\Delta T}}. \quad (1)$$

Here, the parameters ω_0 and ω_1 represent the top (frequency at lowest T) and bottom (frequency at highest T) of the fitted sigmoidal curve, T_0 is the center point, and ΔT controls the width of the curve.

On careful observation, we note that the four modes SP1–SP4 show varying degrees of deviation from the usual anharmonic behavior below T_N, which also depends on the flake thickness. This deviation from anharmonicity can be attributed to SP coupling. Modes SP3 and SP4 show anomalous softening for the FL samples below T_N, whereas the bulk samples show no deviation at all. These modes do not involve vibration of Fe atoms, as shown in the first-principles calculations of vibrational properties in Ref. [30]. SP2, on the other hand, shows deviation from anharmonicity for both bulk and FL cases. This mode involves a small vibration of Fe atoms [30]. The peak SP1 shows deviation from anharmonicity neither for bulk nor for FL. This mode involves large vibrations of the Fe ion [30]. The onset of deviation for each mode remains almost consistent and coincides with the bulk transition temperature K. In addition, the temperature-dependent linewidth, full width at half maximum (FWHM), of all modes shows a shift from monotonic decrease from room temperature at 118 K (see insets of Fig. 3). As a result, the deviation from the anharmonicity is thus indicative of the emergence of AFM order in FL $FePS_3$, and the point of deviation can be identified as the transition temperature (T_N) for the specific layer. Since this onset of deviation remains consistent for both bulk and FL flakes in SP2, one can confirm the retention of AFM order in $FePS_3$ while thinning down to FL [18]. To the best of our knowledge, $FePS_3$ is the only reported 2D magnetic material (AFM-FM) which shows undeviating magnetic transition temperature down to the atomic layers.

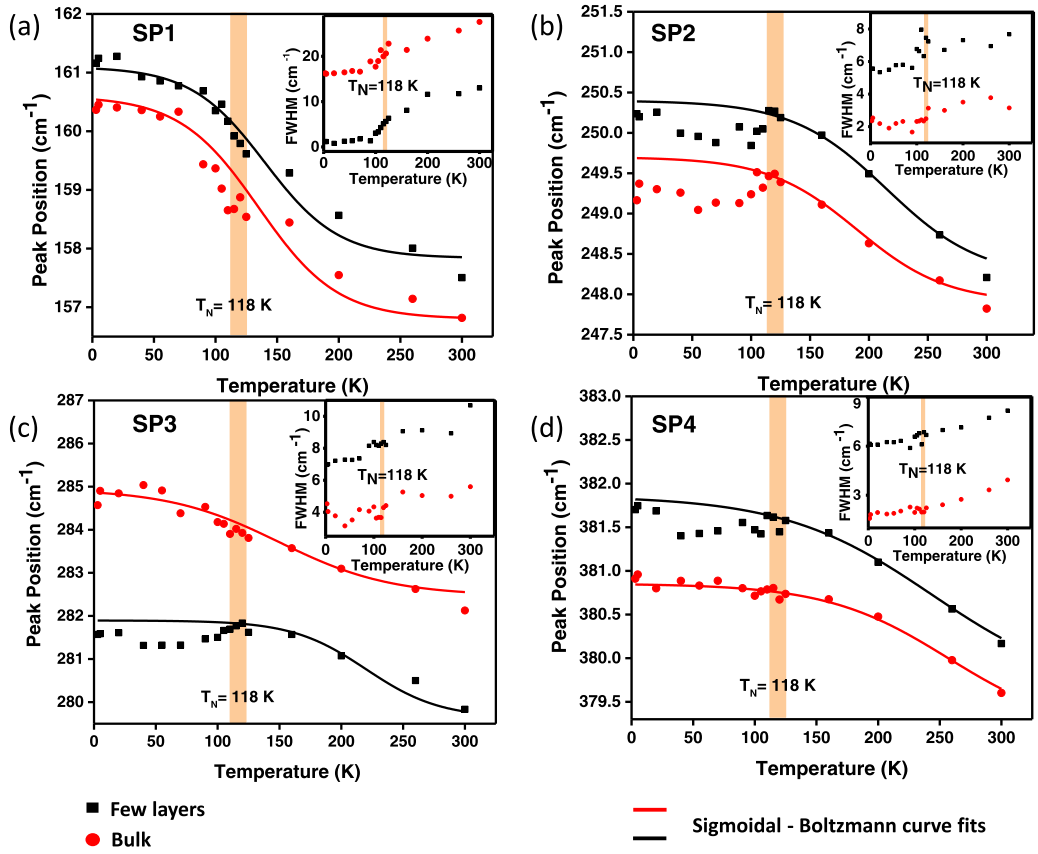

FIG. 3. Spin-phonon (SP) coupling. Temperature dependence (3–300 K) of SP peaks. The symbols, red spheres and black boxes, indicate all measured Raman peaks at different temperatures, whereas the lines show the theoretical anharmonic trend for $FePS_3$ fitted for the experimental data in the given window for bulk and few-layer, respectively. For SP2–SP4 modes (except SP1), there is a deviation from anharmonicity at T_N. The error bars are smaller than the data points. Insets show variation of linewidth with temperature where a discontinuity appears around T_N (bulk and 3L separated by artificial shift). Strength of the SP coupling can be correlated with the projected density of states for each element in the phonon dispersion curve reported in Ref. [35]. The contribution of sulphur in the P_2S_6 cluster compared with divalent Fe^{2+} might be crucial for the SP coupling.

Theoretically, SP coupling introduces exchange interaction between spins and lattice in the total Hamiltonian and can be expressed as $H_{\text{sp-ph}} = \sum_{\alpha\mathbf{q}} \frac{\partial H_{\text{spin}}}{\partial Q_{\alpha\mathbf{q}}} Q_{\alpha\mathbf{q}}$, where $\mathbf{q}$ is the set of reciprocal lattice vectors and $Q_{\alpha\mathbf{q}}$ is the ionic displacement for a phonon with a frequency $\omega_{\alpha\mathbf{q}}$. In a phenomenological description, weak SP coupling in the lattice can be described as [37]

$$\Delta\omega = \lambda_{\text{sp}} \langle S_i S_{i+1} \rangle = -\lambda_{\text{sp}} S^2 \phi(T) \tag{2}$$

where λ_{sp} is the coefficient of SP coupling and $\phi(T)$ is the order parameter given by $\phi(T) = 1 - (T/T_n)^{\gamma}$, and $S = 2$.

The nature of normalized deviation ($\Delta\omega$) as a function of reduced temperature (T/T_N) can be well described by the order parameter γ [37]. From Eq. (1), we can estimate the SP coupling parameter λ_{sp} which varies between 0.10 and 0.15 cm^{-1} for the different modes and thicknesses of flakes. The values of fitting parameter γ and the corresponding λ_{sp} are given in Table I. Unlike magnetic nanoparticles, such as Cr_2O_3, with a large value of SP coupling ($\approx$6 cm^{-1}) [38], λ_{sp} values for $FePS_3$ are small and well in agreement with 2D magnets, like $CrSiTe_3$ and $Cr_2Ge_2Te_6$ [36,37]. Weak SP coupling is essential for the spin transport in 2D magnetic heterostructures, as the scattering from the phonon impurities and perturbations can affect the device performance.

In the mean-field approximations, one can relate $\Delta\omega$ to magnetization as $\Delta\omega(T) \propto \frac{M^2(T)}{M^2_{\text{max}}}$. Figure 4 shows a similar trend in extracted $\Delta\omega(T)$ data from Raman scattering for SP3 and $\frac{M^2(T)}{M^2_{\text{max}}}$ data ($T < T_N$) as obtained from bulk susceptibility measurements. Note that the lifetime ($\tau_{\text{sp}} = \frac{h}{\Gamma_{\text{FWHM}}}$) of the spin-coupled phonon decreases as λ_{sp} increases (inset

TABLE I. Values of λ_{sp} and γ for different modes.

Mode (cm^{-1})	Layer	λ_{sp} (cm^{-1})	γ
	FL	0.097	1.81
380	Bulk	–	–
	FL	0.16	2.89
285	Bulk	–	–
	FL	0.12	4.09
250	Bulk	0.15	4.89
	FL	–	–
150	Bulk	–	–

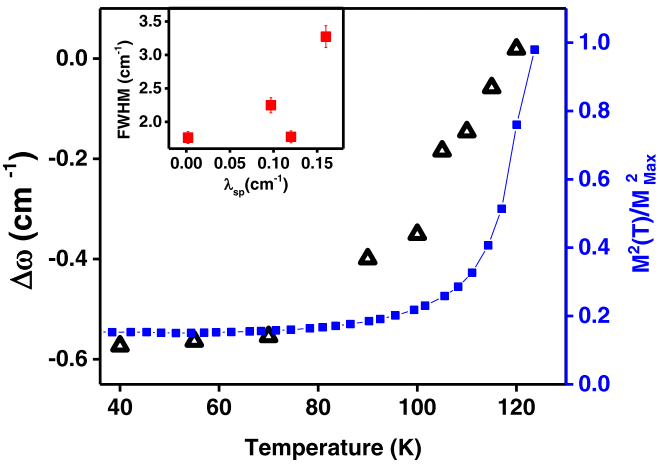

FIG. 4. Deviation from anharmonicity can be correlated to the abrupt jump of magnetization at T_N. The black triangles denote the $\Delta\omega$ values obtained from the shift in Raman modes, while the blue joined dots represent the normalized $M(T)^2$ values as obtained from magnetization measurements. $\Delta\omega$ follows a similar trend as normalized $M(T)^2$. Inset shows the dependence of linewidth with the strength of spin-phonon coupling as calculated from Fig. 3 and Table I.

of Fig. 4). As the temperature is lowered, around 12 K, the frequency of the SP modes goes back to its phononlike usual behavior. This is in contrast to spin-chain cuprates, where impurities become strong scatterers at low temperature (SP mean-free path, $\lambda_{\rm mp} \sim \frac{1}{T}$) [39].

B. Zone-folded phonons (ZPs)

At or below T_N, for bulk and FL, three distinct peaks arise at 88 cm (ZP1), 95 $\rm cm^{-1}$ (ZP2), and 108 $\rm cm^{-1}$ (ZP3) from a single broad peak at 105 $\rm cm^{-1}$ [see Fig. 5(a)]. Strong enhancement in intensity but no considerable change in peak position can be observed in the temperature window $T < T_N$. Quantitatively, the standard deviations of these peaks are in the range 0.22–0.29 $\rm cm^{-1}$ for the FL and 0.07–0.38 $\rm cm^{-1}$ for the bulk, which is much smaller than those of the SP coupled peaks, as depicted in Fig. 5(a)–5(b). Interestingly, for SP peaks (for example, SP2), the change in peak position below T_N is not so abrupt as compared with these three peaks. Considering the spin-dependent Raman scattering, which relates the reduced Raman intensity to the nearest-neighbor correlation function ($\frac{\langle S_0 S_1\rangle}{S^2}$), one can reproduce the abrupt increase of the Raman intensity and the better fit than in SP coupled peaks with typical M^2 dependence [40,41]. As the magnetic order sets in, due to the fact that the magnetic superstructure is double that of a crystallographic cell, the phonon dispersion gets folded [30]. Note that selected area diffraction patterns from high-resolution transmission electron microscopy clearly show that magnetic ordering does not introduce any new diffraction spot [42]. From the phonon dispersion reported in Ref. [30], the mode ZP3 originating from the vibration of Fe atoms can be held responsible for the perturbation, as it belongs to the M point. The zone folding with high Raman response at magnetic transition temperature occurs when the M point folds into the center of the crystallographic Brillouin zone. In addition, the broad peak at 105 $\rm cm^{-1}$ with a width of 20 $\rm cm^{-1}$ is suggestive of electron-phonon coupling at high temperature ($T > T_N$) [see Fig. 5(a)]. Similar to colossal magnetoresistive (CMR) materials [43], here, the interaction between electronic background and phonons at high temperature can be due to low-frequency diffusive hopping of charge carriers. In the paramagnetic phase, the width of the broad peak reduces as the scattering rate ($\frac{1}{\tau_{ZP}}$) decreases with decreasing temperature. Zone-boundary-phonon mode at low temperature and the associated contribution of disorder-induced scattering at high temperature can be important to realize pressure-induced metal-insulator transition and SC in AFM $FePS_3$ [44]. A possible mechanism for the enhancement of intensities at lower temperature may come due to the variation of the d electron transfer with lattice vibrations. The broad peak in our measurement could be related to electronic transitions from the splitting of spin-polarized subbands [45].

C. Magnon

At about $T_N/2$ ($T_M \sim 60$ K), a new peak evolves around 122 $\rm cm^{-1}$ (~3.6 THz) for both bulk and FL samples, which

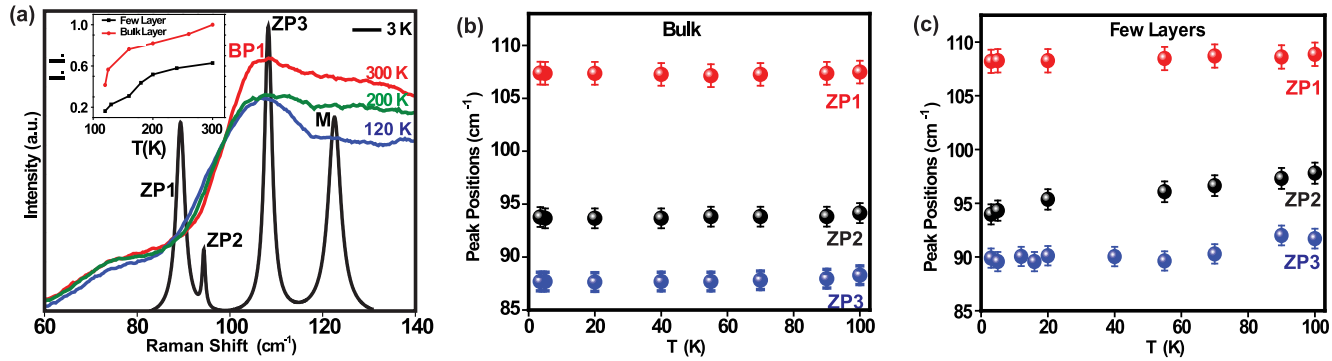

FIG. 5. Zone-folded phonons (ZP). (a) Temperature dependence of the broad peak at 105 $\rm cm^{-1}$. Integrated Raman intensity obtained in the temperature window 120–300 K shows a gradual increase in temperature for bulk and few-layer $FePS_3$. A bosonic background with electronic contribution from spin-disorder scattering can be predicted. Sharp ZP peaks (88, 95, and 108 $\rm cm^{-1}$) with magnon (M) peak [see Sec. III C] can be observed at 3 K in place of the high temperature broad peak. (b) and (c) show the temperature evolution of ZP1–ZP3 peaks for bulk and few-layer samples, respectively.

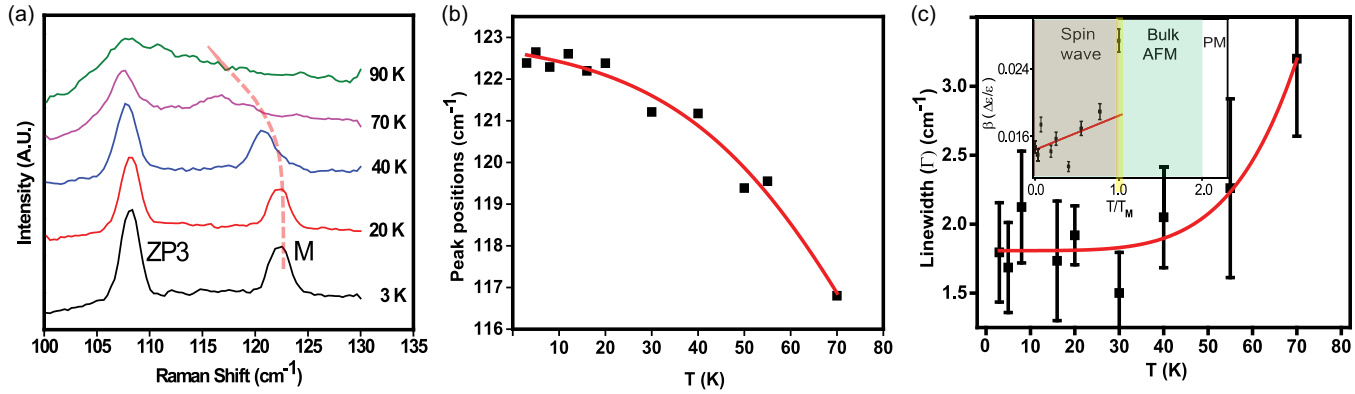

FIG. 6. Magnon mode. (a) and (b) Temperature dependence (3–90 K) of magnon (M) for few-layer samples. Above 70 K, the peak disappeared completely. Red dotted line is guide to the eye for the shift as a function of temperature. In (b), normalized peak positions are shown, which remain constant up to 15 K but redshift as the temperature is increased. (c) Temperature-dependent linewidth of the M peak follows a shifted power law ($\sim T^{3.4}$) nature [51]. Inset shows variation of the dimensionless magnon decay parameter $\beta = \frac{\Delta\epsilon}{\epsilon}$ as temperature increases. Note that a simple linear fit implies the damping of magnon excitation below magnon temperature $T > T_M$ [55].

is identified as the magnon peak (M) [46–49]. It is important to note that the peak is more prominent in the FL than in the bulk. The evolution of this peak as a function of temperature ($T < T_M$) is shown in Fig. 6(a). Interestingly, at high temperature, ZP3 phonons become really close ($\Delta\omega_{M\text{-}ZP} \sim 9\ \text{cm}^{-1}$) to M mode. The position of the M peak remains almost constant at low temperature (until ~15 K). With increasing temperature, it gets blueshifted and subsequently disappears completely at 60 K [see Fig. 6(b)]. The most closely related experimental work on the magnon mode of $FePS_3$ also shows a similar result [49]. The temperature dependence of the M peak has been fitted to the expression used in Eq. (1). A notable blueshift (8 cm^{-1}) of the magnon mode as a function of temperature can be observed as also reported in Ref. [49]. The attenuation of the magnon spin conductivity with temperature, already observed in conventional yttrium-iron garnet (YIG), might explain this nontypical shift compared with usual phonon or SP peaks [50]. Moreover, the integrated intensity of the magnon peak as a function of temperature below the transition temperature follows $(T_M - T)^{0.5}$ behavior, as expected for an order-parameterlike function (not shown here) [49]. The temperature-dependent linewidth of the magnon peak (Γ_M) shows a steep decrease [see Fig. 6(c)]. Within the Hartree-Fock approximation, at small temperature regime, the linewidth of the magnon is predicted to follow a T^4 behavior for the cubic lattice [51]. A magnon in $FePS_3$, on the other hand, follows a $T^\alpha(\alpha \sim 3.4)$ behavior with a constant shift. This constant shift can be attributed to quantum fluctuations beyond Hartree-Fock that lead to a negative part of self-energy. The upper bound of the lifetime of the magnon, as calculated from the linewidth ranging from 5 to 10 ps, corroborates the results as reported in Ref. [49]. The lifetime of the magnon is at least 10 times larger than the temporal period of the magnon (~0.3 ps) [52,53]. This is important for future experiments on coherent control of the terahertz magnon in antiferromagnets [49,52]. Note that the lifetime includes effects from boundary scattering of magnons, magnon-magnon scattering, magnon-phonon scattering, and magnon-magnetic defect scattering [54]. To speculate the behavior of damping of magnons below T_M, thermal effects on both magnon energy (ϵ) and linewidth ($\Delta\epsilon$) can be considered in a phenomenological dimensionless parameter $\beta = \frac{\Delta\epsilon}{\epsilon}$. From the temperature dependence of β [inset in Fig. 6(c)], one can easily point out the low value ($\beta \sim 0.02$ at $\frac{T}{T_N} = 0.8$) compared with ultrathin FM alloys ($\beta \sim 0.4$ at $\frac{T}{T_N} = 0.8$) [55]. In the simplest approximation, a linear fit shows the nature of magnon damping due to possible scattering with impurities and phonons in the lattice, up to T_M [55].

Further, we investigate the AFM magnon mode in the heterostructure formed by different electronic and magnetic phases through proximity effects. Figure 7 shows the low temperature ($T \sim 3$ K) magnon excitation of the heterostructures: FL $FePS_3$ with bulk (i) Bi_2Te_3 and (ii) $Cr_2Ge_2Te_6$. The M mode of $FePS_3$ is highly robust and exists in heterostructures showing proximity-induced effects from other participating 2D materials. It shifts slightly to a lower energy value for $FePS_3/Cr_2Ge_2Te_6$ heterostructures ($\Delta\nu \sim -0.6\,\text{cm}^{-1}$) and to a higher energy value for $FePS_3/Bi_2Te_3$ ($\Delta\nu \sim +0.4\,\text{cm}^{-1}$) as compared with pristine $FePS_3$ flake on SiO_2/Si substrate. A possible explanation of the blueshift of the magnon mode in the case of the heterostructure with Bi_2Te_3 could be due to the band bending and, as a result, the charge transfer that occurs at the $Bi_2Te_3/FePS_3$ interface [56]. Treating the interface as a metal-semiconductor junction, there could be a possible electron transfer out of the $FePS_3$ (indirect band gap of 1.5 eV) into Bi_2Te_3. The electron-rich environment on the surface of Bi_2Te_3 could facilitate the enhancement of AFM transition temperature of $FePS_3$ [56,57]. In addition, we found that change in the peak position ($\Delta\nu$) of SP coupled peaks (SP1–SP4) while cooling from room temperature to 4 K reduces when $FePS_3$ is placed on top of Bi_2Te_3. For example, for the heterostructure, in the case of the SP1 mode, $\Delta\nu$ in the given temperature window is 3.24 cm^{-1} instead of a slightly higher value of 3.41 cm^{-1} in the pristine sample. However, for the SP3 mode, the reduction in the heterostructure is halved from its pristine value.

For a different heterostructure, we have chosen $Cr_2Ge_2Te_6$, which is a FM semiconductor ($T_c \sim 65$ K [14]) with relatively low band gap value (~0.7 eV). The redshift in the magnon

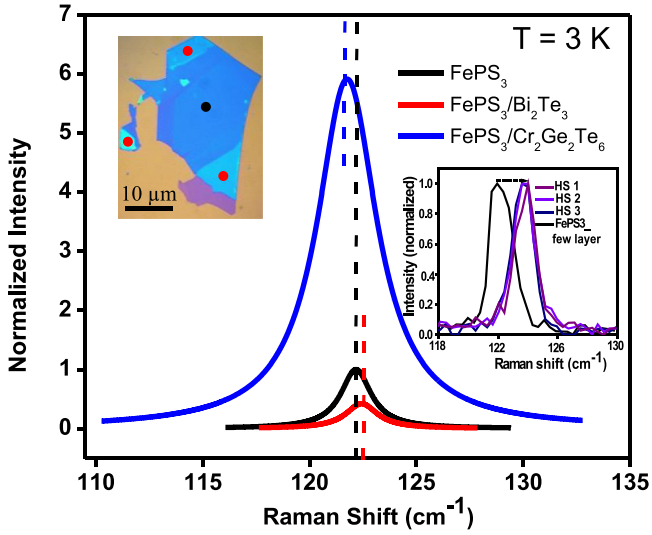

FIG. 7. Magnon modes of $FePS_3$ (black line) in two different heterostructures: $FePS_3/Bi_2Te_3$ in red line and $FePS_3/Cr_2Ge_2Te_6$ in blue line. While a blueshift of magnon mode of pristine $FePS_3$ is observed in the case of the heterostructure containing Bi_2Te_3 ($\Delta\nu \sim 0.4\ cm^{-1}$), a redshift ($\Delta\nu \sim 0.6\ cm^{-1}$) with nearly 6 times increase in intensity can be noticed with $Cr_2Ge_2Te_6$ underneath. Inset (left): Optical image of the van der Waals heterostructure formed by few-layer $FePS_3$ on few-layer Bi_2Te_3 on SiO_2/Si wafer. While the black dot signifies the laser spot on $FePS_3$, red dots indicate three locations of heterostructures for Raman spectroscopy. Scale bar: 10 μm. Inset (right): Shift of characteristic antiferromagnetic magnon peak in few-layer $FePS_3$ with different heterostructures (HS1–3) with Bi_2Te_3. The consistency of the shift indicates the charge transfer in the magnetic heterostructure.

mode of $FePS_3$ in the heterostructure is possibly due to the interfacial hole transfer out of $FePS_3$ into $Cr_2Ge_2Te_6$. Enhancement of the integrated magnon intensity (7 times) could be due to the exchange bias which is commonly observed at the FM-AFM interface [58]. Magnetotransport studies on FL FM-AFM heterostructures are required to draw specific conclusions about the interfacial effects. Heterostructures involving pristine flakes offer clean interfaces, and hence, the underlying physics might be vastly different from the earlier studies on thin films.

IV. CONCLUSIONS

In conclusion, Raman spectroscopy has been utilized as an effective probe that offers insights on magnetic transition, elementary excitations such as spin-lattice coupling, and magnons in FL AFM $FePS_3$. By tracking the temperature evolution of higher energy modes ($>150\ cm^{-1}$), we have confirmed the presence of the AFM order even in FL without any considerable change in the transition temperature ($T_N \sim 120$ K). Adopting a semiclassical approach, strength of the SP coupling has been calculated by going over the deviation from the usual anharmonic phonon behavior. In view of future spintronic devices, weak SP coupling in $FePS_3$ ($\lambda_{sp} \sim 0.15\ cm^{-1}$) makes it an efficient spin-transport layer in the 2D vdW architecture compared with other molecular complexes and magnetic nanoparticles. Also, the presence of a high-temperature electronic background due to spin-disorder scattering ($\sim 105\ cm^{-1}$) and abrupt appearance of three ZPs at or below T_N indicate the possibility of spin-dependent electron-phonon coupling in $FePS_3$. This is crucial for the realization of pressure-induced quenching of spin-ordering and emergence of SC in 2D AFMs. We have identified the AFM magnon ($122\ cm^{-1}$/ 3.6 THz) in $FePS_3$ as reported by McCreary *et al.* [49]. Moreover, monitoring the magnon mode in the vdW heterostructure involving a conventional topological insulator (Bi_2Te_3) and FM semiconductor ($Cr_2Ge_2Te_6$) indicate the effect of interfacial charge transfer. Our results also predict the temperature dependence of the magnon damping in $FePS_3$, which can be a crucial piece of information for future applications such as data processing and communication.

ACKNOWLEDGMENTS

The financial support from IACS and S.D. acknowledges the funding from the Science and Engineering Research Board (SERB), Government of India (Grant No. ECR/2017/002037). SD acknowledges support from the Technical Research Centre (TRC), IACS, Kolkata. The authors are thankful to facilities at UGC-DAE-CSR-Indore. UGC-DAE-CSR Grant No. CRS-M-279 has been utilized for the procurement of the bulk crystal of $FePS_3$. The authors are also grateful to Dr. Vasant Sathe, Prof. Krishnendu Sengupta, Prof. Abhishek Dey, Dr. Kapildeb Dolui, and Dr. Manas Ghosh for useful discussions. The authors declare no competing financial interest.

[1] D. Mermin and H. Wagner, Absence of Ferromagnetism or Antiferromagnetism in One or Two Dimensional Isotropic Heisenberg Models, Phys. Rev. Lett. **17**, 1133 (1966).

[2] L. Onsager, Crystal statistics. I. A two-dimensional model with an order-disorder transition, Phys. Rev. **65**, 117 (1944).

[3] J. L. Lado and J. Fernández-Rossier, On the origin of magnetic anisotropy in two dimensional CrI_3, 2D Mater. **4**, 035002 (2017).

[4] C. S. Arnold, M. Dunlavy, and D. Venus, Magnetic susceptibility measurements of ultrathin films using the surface magneto-optic Kerr effect: optimization of the signal-to-noise ratio, Rev. Sci. Instrum. **68**, 4212 (1997).

[5] T. Nakagawa and T. Yokoyama, Magnetic Circular Dichroism near the Fermi Level, Phys. Rev. Lett. **96**, 237402 (2006).

[6] C. Gong and X. Zhang, Two-dimensional magnetic crystals and emergent heterostructure devices, Science **363**, eaav4450 (2019).

[7] K. S. Novoselov, A. K. Geim, S. V. Morozov, D. Jiang, Y. Zhang, S. V. Dubonos, I. V. Grigorieva and A. A. Firsov, Electric field effect in atomically thin carbon films, Science **306**, 666 (2004).

[8] A. Candini, S. Klyatskaya, M. Ruben, W. Wernsdorfer, and M. Affronte, Graphene spintronic devices with molecular nanomagnets, Nano Lett. **11**, 2634 (2011).

[9] D. Xiao, G.-B. Liu, W. Feng, X. Xu, and W. Yao, Coupled Spin

and Valley Physics in Monolayers of MoS_2 and Other Group-VI Dichalcogenides, Phys. Rev. Lett. **108**, 196802 (2012).

[10] A. Banerjee, J. Yan, J. Knolle, C. A. Bridges, M. B. Stone, M. D. Lumsden, D. G. Mandrus, D. A. Tennant, R. Moessner, and S. E. Nagler, Neutron scattering in the proximate quantum spin liquid α-$RuCl_3$, Science **356**, 1055 (2017).

[11] N. Chandrasekharan and S. Vasudevan, Magnetism and exchange in the layered antiferromagnet $NiPS_3$, J. Phys.: Condens. Matter **6**, 4569 (1994).

[12] K. Kurosawa, S. Saito, and Y. Yamaguchi, Neutron diffraction study on $MnPS_3$ and $FePS_3$, J. Phys. Soc. Jpn. **52**, 3919 (1983).

[13] B. Huang, G. Clark, E. Navarro-Moratalla, D. R. Klein, R. Cheng, K. L. Seyler, D. Zhong, E. Schmidgall, M. A. McGuire, D. H. Cobden, W. Yao, D. Xiao, P. J. Herrero, and X. Xu, Layer-dependent ferromagnetism in a van der Waals crystal down to the monolayer limit, Nature **546**, 270 (2017).

[14] C. Gong, L. Li, Z. Li, H. Ji, A. Stern, Y. Xia, T. Cao, W. Bao, C. Wang, Y. Wang, Z. Q. Qiu, R. J. Cava, S. G. Louie, J. Xia, and X. Zhang, Discovery of intrinsic ferromagnetism in two-dimensional van der Waals crystals, Nature **546**, 265 (2017).

[15] S. Jiang, J. Shan, and K. F. Mak, Electric-field switching of two-dimensional van der Waals magnets, Nat. Mater. **17**, 406 (2018).

[16] Z. Fei, B. Huang, P. Malinowski, W. Wang, T. Song, J. Sanchez, W. Yao, D. Xiao, X. Zhu, A. F. May, W. Wu, D. H. Cobden, J.-H. Chu, and X. Xu, Two-dimensional itinerant ferromagnetism in atomically thin Fe_3GeTe_2, Nat. Mater. **17**, 778 (2018).

[17] S. Chen, C. Huang, H. Sun, J. Ding, P. Jena, and E. Kan, Boosting the Curie temperature of two-dimensional semiconducting CrI_3 monolayer through van der Waals heterostructures, J. Phys. Chem. C **123**, 17987 (2019).

[18] M. Gibertini, M. Koperski, A. F. Morpurgo, and K. S. Novoselov, Magnetic 2D materials and heterostructures, Nat. Nanotechnol. **14**, 408 (2019).

[19] W. Han, Y. Otani, S. Maekawa, Quantum materials for spin and charge conversion, npj Quant. Mater. **3**, 27 (2018).

[20] L. Šmejkal, Y. Mokrousov, B. Yan, and A. H. MacDonald, Topological antiferromagnetic spintronics, Nat. Phys. **14**, 242 (2018).

[21] K. S. Burch, D. Mandrus, and J. Park, Magnetism in two-dimensional van der Waals materials, Nature **563**, 47 (2018).

[22] A. C. Ferrari and D. M. Basko, Raman spectroscopy as a versatile tool for studying the properties of graphene, Nat. Nanotechnol. **8**, 235 (2013).

[23] Xin Cong, X.-L. Liu, M.-L. Lin, and P.-H. Tan, Application of Raman spectroscopy to probe fundamental properties of two-dimensional materials, npj 2D Mater. Appl. **4**, 13 (2020).

[24] A. C. Ferrari, J. C. Meyer, V. Scardaci, C. Casiraghi, M. Lazzeri, F. Mauri, S. Piscanec, D. Jiang, K. S. Novoselov, S. Roth, and A. K. Geim, Raman Spectrum of Graphene and Graphene Layers, Phys. Rev. Lett. **97**, 187401 (2006).

[25] W. Xing, L. Qiu, X. Wang, Y. Yao, Y. Ma, R. Cai, S. Jia, X. C. Xie, and Wei Han, Magnon Transport in Quasi-Two-Dimensional van der Waals Antiferromagnets, Phys. Rev. X **9**, 011026 (2019).

[26] Q. Zhang, M. An, S. Yuan, Y. Wu, D. Wu, J. Luo, N. Wang, W. Bao, and Y. Wang, Phonon softening and forbidden mode in $Na_{0.5}CoO_2$ observed by Raman scattering, Phys. Rev. B **77**, 045110 (2008).

[27] Y. Du, G. Qiu, Y. Wang, M. Si, X. Xu, W. Wu, and P. D. Ye, One-dimensional van der Waals material tellurium: Raman spectroscopy under strain and magneto-transport, Nano Lett. **17**, 3965 (2017).

[28] A. McCreary, T. T. Mai, F. G. Utermohlen, J. R. Simpson, K. F. Garrity, X. Feng, D. Shcherbakov, Y. Zhu, J. Hu, D. Weber, K. Watanabe, T. Taniguchi, J. E. Goldberger, Z. Mao, C. N. Lau, Y. Lu, N. Trivedi, R. Valdés Aguilar, and A. R. Hight Walker, Distinct magneto-Raman signatures of spin-flip phase transitions in CrI_3, Nat. Commun. **11**, 3879 (2020).

[29] X. Wang, K. Du, Y. Y. F. Liu, P. Hu, J. Zhang, Q. Zhang, M. H. S. Owen, X. Lu, C. K. Gan, P. Sengupta, C. Kloc, and Q. Xiong, Raman spectroscopy of atomically thin two-dimensional magnetic iron phosphorus trisulfide ($FePS_3$) crystals, 2D Mater. **3**, 031009 (2016).

[30] J.-U. Lee, S. Lee, J. H. Ryoo, S. Kang, T. Y. Kim, P. Kim, C.-H. Park, J.-G. Park, and H. Cheong, Ising-type magnetic ordering in atomically thin $FePS_3$, Nano Lett. **16**, 7433 (2016).

[31] K. Kim, S. Y. Lim, J.-U. Lee, S. Lee, T. Y. Kim, K. Park, G. S. Jeon, C.-H. Park, J.-G. Park, and H. Cheong, Suppression of magnetic ordering in XXZ-type antiferromagnetic monolayer $NiPS_3$, Nat. Commun. **10**, 345 (2019).

[32] K. Kim, S. Y. Lim, J. Kim, J.-U. Lee, S. Lee, P. Kim, K. Park, S. Son, C.-H. Park, J.-G. Park, and H. Cheong, Antiferromagnetic ordering in van der Waals 2D magnetic material $MnPS_3$ probed by Raman spectroscopy, 2D Mater. **6**, 041001 (2019).

[33] R. de Sousa and J. E. Moore, Optical coupling to spin waves in the cycloidal multiferroic $BiFeO_3$, Phys. Rev. B **77**, 012406 (2008)

[34] A. Castellanos-Gomez, M. Buscema, R. Molenaar, V. Singh, L. Janssen, H. S. J. van der Zant, and G. A. Steele, Deterministic transfer of two-dimensional materials by all-dry viscoelastic stamping, 2D Mater. **1**, 011002 (2014).

[35] A. Hashemi, H.-P. Komsa, M. Puska, and A. V. Krasheninnikov, Vibrational properties of metal phosphorus trichalcogenides from first-principles calculations, J. Phys. Chem. C **121**, 27207 (2017).

[36] L. D. Casto, A. J. Clune, M. O. Yokosuk, J. L. Musfeldt, T. J. Williams, H. L. Zhuang, M.-W. Lin, K. Xiao, R. G. Hennig, B. C. Sales, J.-Q. Yan, and D. Mandrus, Strong spin-lattice coupling in $CrSiTe_3$, APL Mater. **3**, 041515 (2015).

[37] B. H. Zhang, Y. S. Hou, Z. Wang, R. Q. Wu, First-principles studies of spin-phonon coupling in monolayer $Cr_2Ge_2Te_6$, Phys. Rev. B **100**, 224427 (2019).

[38] S. Y. Wu, Application of Raman microscopy for spin-phonon coupling and magnon excitation study in nanocrystals, in *Current Microscopy Contributions to Advances in Science and Technology*, edited by A. Mendez-Vilas (Formatex, Norristown, PA, 2012).

[39] A. L. Chernyshev and A. V. Rozhkov, Heat Transport in Spin Chains with Weak Spin-Phonon Coupling, Phys. Rev. Lett. **116**, 017204 (2016).

[40] L. Zhang, P. F. Guan, D. L. Feng, X. H. Chen, S. S. Xie, and M. W. Chen, Spin-dependent electron-phonon interaction in SmFeAsO by low-temperature Raman spectroscopy, J. Am. Chem. Soc. **132**, 15223 (2010).

[41] A. Fainstein, P. Etchegoin, H. J. Trodahl, and J. L. Tallon, Spin-order-dependent Raman scattering in $RuSr_2GdCu_2O_8$, Phys. Rev. B **61**, 15468 (2000).

[42] C. Murayama, M. Okabe, D. Urushihara, T. Asaka, K. Fukuda, M. Isobe, K. Yamamoto, and Y. Matsushita, Crystallographic features related to a van der Waals coupling in

the layered chalcogenide $FePS_3$, J. Appl. Phys. **120**, 142114 (2016).

[43] S. Merten, O. Shapoval, B. Damaschke, K. Samwer, and V. Moshnyaga, Magnetic-field-induced suppression of Jahn-Teller phonon bands in $(La_{0.6}Pr_{0.4})_{0.7}Ca_{0.3}MnO_3$: the mechanism of colossal magnetoresistance shown by Raman spectroscopy, Sci. Rep. **9**, 2387 (2019)

[44] Y. Wang, J. Ying, Z. Zhou, J. Sun, T. Wen, Y. Zhou, N. Li, Q. Zhang, F. Han, Y. Xiao, P. Chow, W. Yang, V. V. Struzhkin, Y. Zhao, and H.-k. Mao, Emergent superconductivity in an iron-based honeycomb lattice initiated by pressure-driven spin-crossover, Nat Commun **9**, 1914 (2018).

[45] G. Benedek and A. Frey, Lattice dynamics in layered transition-metal dihalides, Phys. Rev. B **21**, 2482 (1980).

[46] T. Sekine, M. Jouanne, C. Julien, and M. Balkanski, Light-scattering study of dynamical behavior of antiferromagnetic spins in the layered magnetic semiconductor $FePS_3$, Phys. Rev. B **42**, 8382 (1990).

[47] A. R. Wildes, M. E. Zhitomirsky, T. Ziman, D. Lançon, and H. C. Walker, Evidence for biquadratic exchange in the quasi-two-dimensional antiferromagnet $FePS_3$, J. Appl. Phys. **127**, 223903 (2020).

[48] A. R. Wildes, K. C. Rule, R. I. Bewley, M. Enderle, and T. J. Hicks, The magnon dynamics and spin exchange parameters of $FePS_3$, J. Phys.: Condens. Matter **24**, 416004 (2012).

[49] A. D. McCreary, J. R. Simpson, T. T. Mai, R. D. McMichael, J. E. Douglas, N. P. Butch, C. L. Dennis, R. V. Aguilar, and A. R. Hight Walker, Quasi-two-dimensional magnon identification in antiferromagnetic $FePS_3$ via magneto-Raman spectroscopy, Phys. Rev. B **101**, 064416 (2020).

[50] L. J. Cornelissen, J. Shan, and B. J. van Wees, Temperature dependence of the magnon spin diffusion length and magnon spin conductivity in the magnetic insulator yttrium iron garnet, Phys. Rev. B **94**, 180402(R) (2016).

[51] E. Balcar, Spin-wave lifetime in antiferromagnets, J. Phys. Colloques **32**, C1-701 (1971).

[52] W. Jin, H. H. Kim, Z. Ye, S. Li, P. Rezaie, F. Diaz, S. Siddiq, E. Wauer, B. Yang, C. Li, S. Tian, K. Sun, H. Lei, A. W. Tsen, L. Zhao, and R. He, Raman fingerprint of two terahertz spin wave branches in a two-dimensional honeycomb Ising ferromagnet, Nature Comm. **9**, 5122 (2018).

[53] S. Rosenblum, A. H. Francis, and R. Merlin, Two-magnon light scattering in the layered antiferromagnet $NiPS_3$: spin-1/2-like anomalies in a spin-1 system, Phys. Rev. B **49**, 4352 (1994).

[54] S. Yoon, H. L. Liu, G. Schollerer, S. L. Cooper, P. D. Han, D. A. Payne, S.-W. Cheong, and Z. Fisk, Raman and optical spectroscopic studies of small-to-large polaron crossover in the perovskite manganese oxides, Phys. Rev. B **58**, 2795 (1998).

[55] H. J. Qin, Kh. Zakeri, A. Ernst, and J. Kirschner, Temperature Dependence of Magnetic Excitations: Terahertz Magnons above the Curie Temperature, Phys. Rev. Lett. **118**, 127203 (2017).

[56] G. B. Osterhoudt, R. Carelli, K. S. Burch, F. Katmis, N. Gedik, and J. S. Moodera, Charge transfer in EuS/Bi_2Se_3 heterostructures as indicated by the absence of Raman scattering, Phys. Rev. B **98**, 014308 (2018).

[57] F. Katmis, V. Lauter, F. S. Nogueira, B. A. Assaf, M. E. Jamer, P. Wei, B. Satpati, J. W. Freeland, I. Eremin, D. Heiman, P. Jarillo-Herrero, and J. S. Moodera, A high-temperature ferromagnetic topological insulating phase by proximity coupling, Nature **533**, 513 (2016).

[58] W. S. Lew, A. Ercole, G. Lauhoff, E. T. M. Kernohan, J. Lee, and J. A. C. Bland, Temperature dependence of spin waves in Co/CoO bilayers, J. Appl. Phys. **89**, 7654 (2001).